CELLULAR INSTABILITY PHENOMENON IN PREMIXED TUBULAR FLAMES AND NON-PREMIXED OPPOSED TUBULAR FLAMES

By

Yu Wang

Thesis

Submitted to the Faculty of the

Graduate School of Vanderbilt University

in partial fulfillment of the requirements

for the degree of

MASTER OF SCIENCE

in

Mechanical Engineering

December, 2008

Nashville, Tennessee

Approved:

Professor Robert W. Pitz

Professor Deyu Li

Professor Kenneth A. Debelak

ACKNOWLEDGEMENTS

I appreciate all of those who help me complete this thesis. First and foremost, I would like to express thankfulness to my advisor, Dr. Pitz, for his careful guidance and sincere help. Valuable help from fellow graduate students Dr. Shengteng Hu and Dr. Peiyong Wang is also highly appreciated.

This work is sponsored by National Science Foundation Grant No. CTS-0314704 with Phillip Westmoreland as the program manager. RWP acknowledges the support of NASA Grant No. NNC04AA14A with John Brooker as the technical monitor to develop the new tubular burner and appreciates the loan of the Xybion camera from NASA Glen Research Center.

TABLE OF CONTENTS

Page

LIST OF TABLES

Table Page

LIST OF FIGURES

CHAPTER I

INTRODUCTION

Cellular instability is a significant phenomenon in flame study. It has been found with many different types of premixed and non-premixed flames, such as, a stripped structure in a premixed stagnation point flame burner, a unburned region in a Bunsen burner, and cellular structure in the axisymmetric jet flame. Although their appearance or structure are different, all of them have been believed to be associated with thermal-diffusive effects that depend on Lewis number (the ratio of the thermal diffusivity to the deficient reactant mass diffusivity), hydrodynamic effects that depends on density change in premixed flames, the equivalence ratio (for premixed flames), and the initial mixture strength (for non-premixed flames). In addition, stretch rate, curvature, and pressure could influence the flame in the specific burners used.

The tubular flame is one kind of combustion configuration where the spatial shape looks like a round tube. Reactants are generally fed in along the radial direction and products exit the combustion region along the direction of tube axis (see Figure 1). Depending on the configuration of the reactants streams, the tubular flame is categorized to be a premixed and non-premixed. The typical flow fields for both cases are showed in Figure 1.

Recently, the research work about instability on premixed tubular flames and

non-premixed opposed tubular flame has been received more attention. A series of experiments were conducted in various tubular burners by different researchers. But a systematic explanation about the intrinsic factors and physical mechanisms that dominate the unstable flame behavior is still needed. This thesis intends to present the experimental work on the parameter space of the instabilities and explain the physical mechanism for the instabilities.

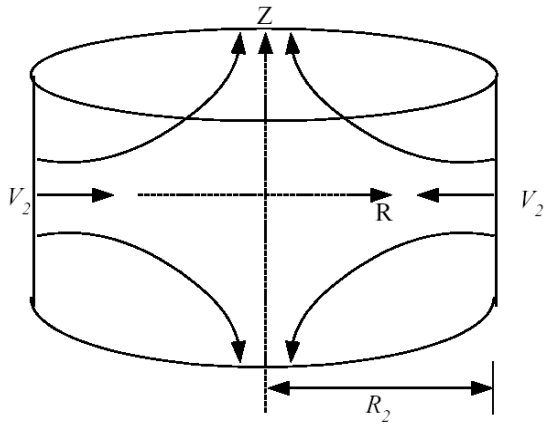

(a) Premixed tubular flame flow field

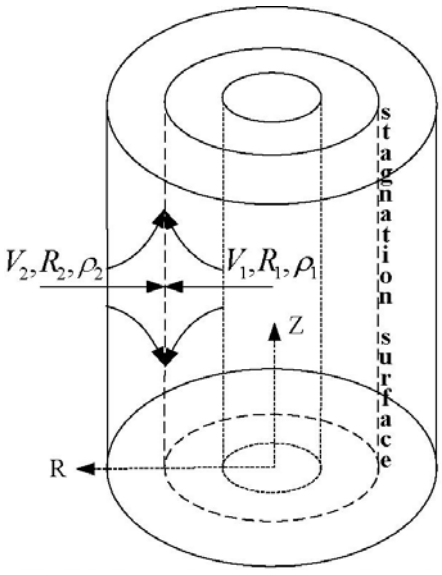

(b) Non-premixed opposed tubular flame flow field

Figure 1. Typical flow field of premixed tubular flame and non-premixed opposed tubular flame.

CHAPTER II

CELLULAR INSTABILITY AND EXTINCTION IN PREMIXED TUBULAR FLAMES

Introduction

The stretch effect is one of the main causes of flame extinction (Williams 1981) and comprehensive reviews have been given (Law et al. 1998, Law and Sung 2000) on the stretch effect in premixed flames. One type of stretched flame, the premixed tubular flame, has also been carefully investigated both theoretically and experimentally (Ishizuka et al. 1993). Wang et al. (2006) derived the definition of the stretch rate for the premixed and non-premixed tubular flames. Using the laser diagnostic method, Mosbacher et al. (2002) and Hu et al. (2006) investigated the effect of stretch on lean H_2/air, CH_4/air and C_3H_8/air premixed tubular flames and compared extinction limit data from experiments with that from numerical simulations. Ishizuka (1984, 1989 and 1991), Sakai and Ishizuka (1992), using tubular burners with rotating and non-rotating flows, conducted a series of experiments to study the behavior of the premixed tubular flames at near–extinction conditions. They indicated that, at the extinction point, the flame of lean hydrogen/air or methane/air flame, whose Lewis number is less than one, shows a small diameter and is almost converted into a luminous rod. On the other hand, the rich methane flame whose Lewis number is greater than one, cannot reach such a small diameter at the extinction point. Tubular flames were found to have a slightly larger flammable range than the

standard flammability range (Ishizuka 1993 and 1991). Ishizuka indicated that the effect of stretch rate, fuel concentration and Lewis number on the tubular flame were important in these phenomenon. Also, Ishizuka (1991) increasingly dilutes the air with nitrogen in lean methane and propane/air tubular flames, leading to increased fuel/O_2 ratios, and finds that the fuel mole fraction is almost constant at the lean limit for each respective fuel.

Cellular instability is another interesting feature in premixed flames and was recently reviewed by Matalon (2007) and Law (2006). It generally accepted that flame stretch stabilizes instabilities in premixed flames and if instabilities are found, they occur in the coordinate direction that has the least amount of flame stretch. Law (2006) showed images of instabilities appearing along radial lines in a rich butane-air axisymmetric stagnation point flow "star" flame measured (Lee and Sohrab 1995). The instabilities were arranged symmetrically like a "star" along the azimuthal coordinate of the flame surface and these star instabilities disappeared at high stretch rate. Star shaped flames are also reported in an axisymmetric counterflow burner (Ishizuka and Law 1982). Ishizuka (1993, 1991) observed cellular phenomenon in his tubular premixed flames where petals occurred symmetrically around the tubular flame surface. Tubular flames are stretched in axial direction but not in the angular direction along the circumference of the flame surface. Lee and Sohrab (1995) studied cellular instabilities in a rich premixed butane-air two-dimensional stagnation point flame. The flame was rectangular (8.9 cm long x 2.54 cm wide) and they found parallel cellular flame strips occurred equally spaced in the longer (8.9 cm) direction

that had a lesser amount of stretch.

Previous experiments in tubular premixed flames have mainly focused on air as oxidizer, with the exception of Ishizuka's investigation where he investigated premixed tubular flames with different oxygen concentrations by diluting the air with additional nitrogen. In the previous studies, only nitrogen was used as the diluent. However, flames with other diluents and enriched oxygen are needed to investigate preferential diffusion effects. In this work, premixed tubular flames using H_2/O_2 or CH_4/O_2 mixed with various inert diluents (e.g., Ar, CO_2, N_2) and enriched oxygen are studied to determine their extinction limits and onset conditions for cellular instabilities.

Experimental Setup

All the experiments are conducted in a newly designed tubular burner, shown in Figure 2.

It is similar to the one used by Mosbacher et al. (2002) except two main changes in configuration: a) The premixed combustible gas mixture is introduced to the annular stagnation chamber through two annular porous plates, in order to generate a more uniform flow at the nozzle exit; b) The gas mixture exits through a converging cylindrical nozzle of 12 mm in radius and 8 mm in height. The small height of 8 mm (compared to a 20 mm height Mosbacher et al. 2002) allows higher stretch rates to be studied before the onset of turbulence. Turbulence effects occur when the burner Reynolds number, $Re = VD_h/\nu$ reaches about 2000. Here V is the velocity at the

nozzle exit, D_h, the hydraulic diameter, equals half of the burner height (4 mm in this case), and ν is the kinematic viscosity. The burner has three optical ports perpendicular to each other along the periphery to allow optical access for flame imaging and laser-based diagnostics. A secondary porous nozzle (not installed in these experiments) can be installed along the axis of symmetry to allow non-premixed tubular flames to be produced. Extinction measurement of curved premixed/non-premixed flames will be conducted using this new tubular burner that is vertically mounted as shown in Figure 2. Using this burner, a premixed tubular flame, with the reactants flowing radially inward toward it, is formed around the symmetric axis.

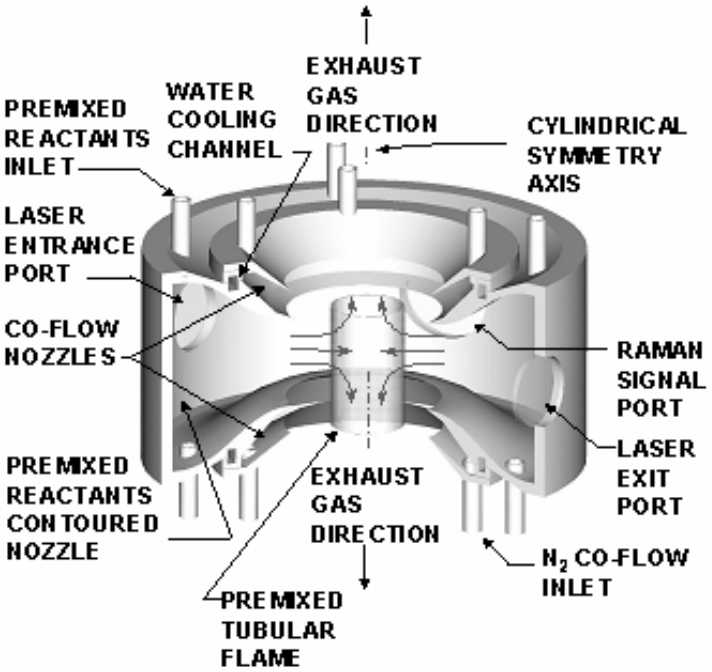

Figure 2. Tubular burner configuration

The extinction and cellular structure of the flame is monitored along the axial

direction with a video camera (60 Hz). First, the axially-integrated chemiluminescence emission from the flames is reflected by a mirror mounted underneath the tubular burner at 45 degrees to the axis of symmetry, which provides an axial view of the vertical tubular flame. Then, the infrared sensitive ICCD video camera (Xybion ISG-250) mounted horizontally toward the mirror collects and records these emissions and transmits them to the display. These videos are also recorded onto a computer for further analysis. A typical picture of a recorded flame is shown in Figure 3.

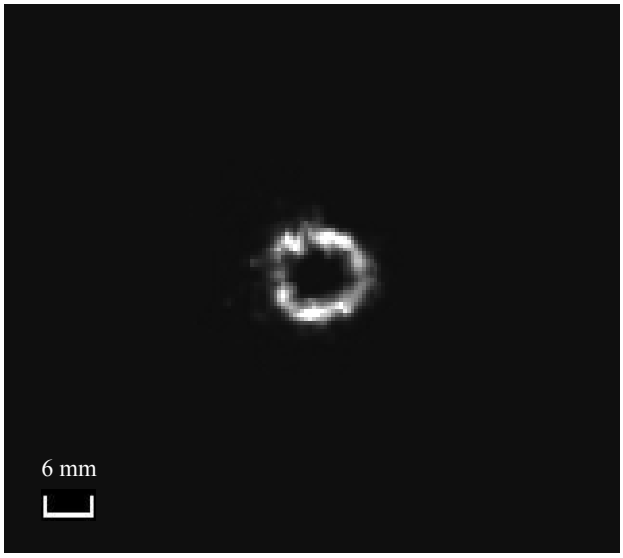

Figure 3. Axial view of a H_2/air tubular flame (Φ=0.2, k=406/s).

In the present work, H_2 or CH_4 mixed with oxidizer flow consisting of oxygen and diluent are used. Here, N_2, CO_2 and Ar are used as diluent; all the experimental conditions are listed in Table 1. The fuel and oxidizer gases are mixed at least 3 meters before entering the tubular burner to ensure adequate premixing. Their flow rates are set separately with fully automated mass flow controllers (Teledyne Hastings

HFC-202/203), whose nominal accuracy is 1% of full scale. Prior to conducting the experiments, the controllers are calibrated with laminar flow elements.

Table 1. List of experimental conditions for premixed tubular flames

Fuel	Oxidizer	Diluent	Concentration	Equivalence Ratio	Stretch Rate (s^{-1})
H_2	O_2	N_2	79%	0.113 - 0.344	16.9 - 639.6
			70%	0.082 - 0.208	25.1 - 668.1
		CO_2	79%	0.155 - 0.44	33.9 - 690.3
			70%	0.105 - 0.29	50.1 - 682.5
		Ar	79%	0.087 - 0.22	19.0 - 659.9
			70%	0.062 - 0.158	49.0 - 660.2
CH_4	O_2	N_2	79%	0.500 - 0.66	25.2 - 758.3
			70%	0.350 - 0.42	25.2 - 670.3
		CO_2	79%	N/A*	N/A*
			70%	0.476 - 0.61	51.1 - 602.6
		Ar	79%	0.361 - 0.42	49.3 - 658.1
			70%	0.270 - 0.30	49.6 - 658.8

* The flame is not initiated ever for an equivalence ratio approaching one.

For extinction experiments, the oxidizer gas flow rate is fixed and the fuel flow rate is decreased gradually (normally 0.1-0.2% of full scale of mass flow controller) until extinction is reached. The recorded flow rate of fuel and oxidizer is repeated at least twice. The mean values are used as the final data.

For cellular instability experiments, the oxidizer gas flow is also kept steady. By increasing the fuel flow rate from near-extinction conditions to a certain point, the cellular phenomenon starts to appear, where the shape of flame is transformed from a perfect circle to multi-petal structure. In our case, 2 to 9 cells are observed. Because more than 7 cells are not observed at every condition and it is hard to distinguish the

transformation from non-cell to 2 cells, only the data for 3-7 cells are reported in this here.

Results and Discussion

Extinction data for different oxidizer-diluent combinations are presented first. The results encompass various diluents with varying concentrations. The experimental results of cellular structure are presented and discussed next. In all experiments, the stretch rate is calculated according to the definition of Wang et al. (2006): $k = \pi V/R$ where R is the radius of the cylindrical nozzle (R = 12 mm). Only single component fuels are studied (either H_2 or CH_4) and the equivalence ratio (Φ) is defined as the mole ratio of fuel-to-oxygen normalized by stoichiometric mole ratio of fuel-to-oxygen (Law 2006).

Extinction behavior

Figure 4 shows the extinction curves of H_2 and CH_4 burning in air (21% O_2 in N_2) and oxygen-enriched air (30% O_2 in N_2). At high stretch rates ($k > \sim 80\ s^{-1}$), the equivalence ratio at extinction increases with the stretch rate. The high stretch rate rapidly removes heat generated by the chemical reaction, so more fuel is required to balance the heat loss in order to avoid extinction. At the same stretch rate, the extinction equivalence ratio for CH_4 is always higher than that for H_2.

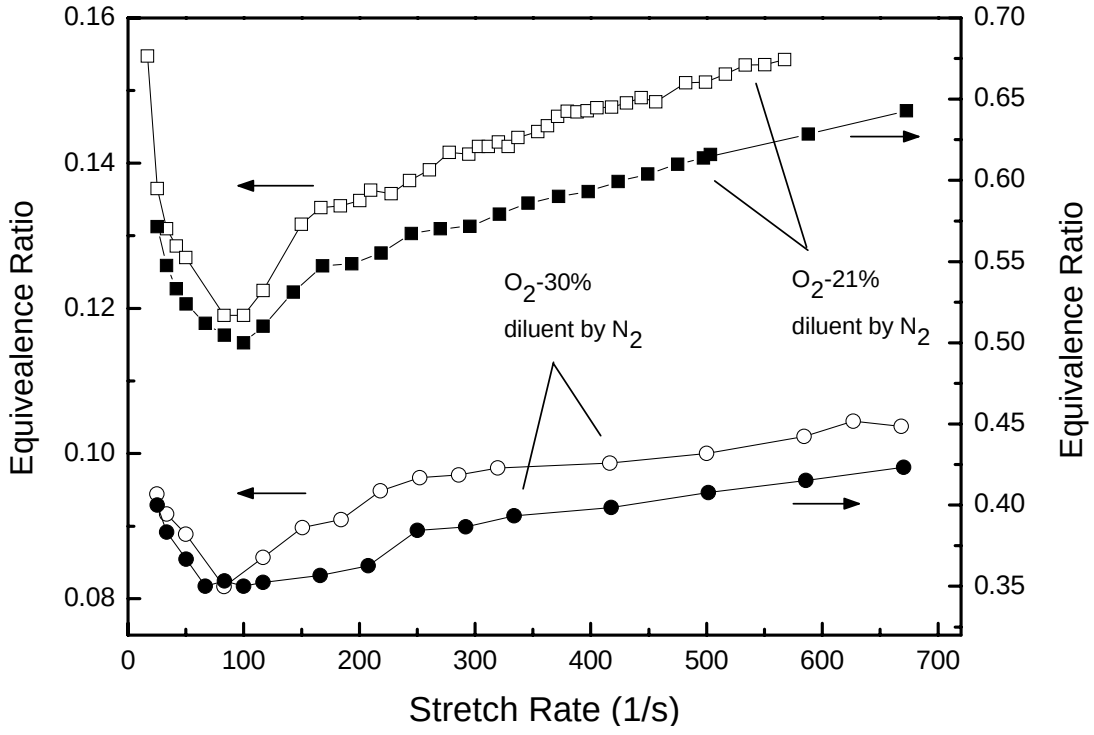

Figure 4. Extinction curves of H_2/air (hollow symbols) and CH_4/air (solid symbols) tubular flames

Increasing the oxygen concentration in the oxidizer flow, the results at different diluent concentrations show that the higher the oxygen concentration is, the lower the extinction equivalence ratio is, correspondingly. The higher oxygen concentration in the oxidizer mixture means less heat goes to the inert gases. As a result, less fuel (hydrogen) is needed to maintain the flame temperature in order to sustain the flame. The similar trend is observed in the CH_4 flame as seen in Figure 4.

Furthermore, when the stretch rate is low (Figure 4), each curve shows a reversed trend, i.e. the extinction equivalence ratio increases with decreasing stretch rate. As Ishizuka (1993) mentioned in his work, heat loss to environment, especially to burner, is responsible for this experimental observation. Ishizuka compared porous wall tubular burners of two diameters (16 mm and 30 mm) and found that the smaller

diameter tubular burner had reduced flammability limits reportedly due to higher heat loss (Ishizuka 1993 and 1991). Also Ju et al. (1999) numerically predicted for CH_4/air tubular flames that as the stretch rate decreases, radiation loss becomes a more significant factor in flame quenching. As the stretch rate is reduced, heat loss becomes more and more dominant, which means more fuel is needed to maintain the flame.

The shapes of the H_2/air and CH_4/air curves (21% O_2 in N_2) shown in Figure 3 are consistent with the shapes of the extinction curves for H_2/air and CH_4/air reported by Ishizuka [1993 and 1991]. Ishizuka measured extinction equivalence ratio[1] in the lower range of stretch rates ($k=7\text{-}43s^{-1}$) for H_2/air and CH_4/air vertically mounted tubular flames and his results clearly show the increase of extinction equivalence ratio at decreased stretch rate ($k<\sim15s^{-1}$) but only show a slight increase in the extinction equivalence ratio at higher stretch rates ($k=15\text{-}43s^{-1}$). Part of H_2/air experimental data from Figure 4 is directly compared to Ishizuka's results in Figure 5. Due to the differences in the burner dimensions and inlet radial velocities, the experimental conditions do not completely overlap. However, based on the available data at the same stretch rates, it can be seen that the present work shows higher extinction equivalence ratios than those from Ishizuka; this increase can be explained by the smaller diameter of the present burner (24 mm) when compared to Ishizuka's burner (30 mm) leading to increased heat loss. Comparing the present results in the CH_4/air tubular flames to Ishizuka's extinction data for vertically mounted CH_4/air tubular

[1] Ishizuka [1991, 1993] actually measured the fuel concentration (% fuel in volume) at extinction versus the mean injected velocity at the porous cylinder wall. These values have been converted to extinction equivalence ratio versus stretch rate for comparison purposes.

flames, the extinction equivalence ratios are also higher than Ishizuka's values, probably due to the smaller diameter of our tubular burner.

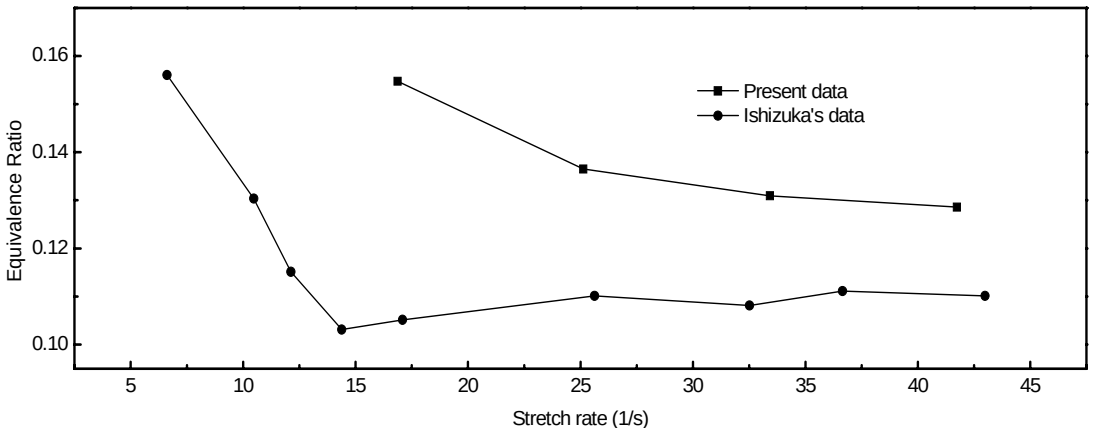

Figure 5. A comparison of the extinction equivalence ratios of H_2/air flames between the current work and Ishizuka's work (1991).

Figure 6 shows the stretch rate versus equivalence ratio at the extinction point for different types of diluents. Similar to N_2, using CO_2 and Ar as diluent, higher oxygen concentration in the oxidizer flow sustains the flame at lower equivalence ratio. Also, for cases in which different diluents have the same concentration, the oxidizer diluted by CO_2 needs more fuel to sustain the flame than either of those diluted by N_2 or Ar. The reason comes from the heat capacity and emissivity of the diluent gas. That is, CO_2 has a higher heat capacity and emissivity compared to Ar and N_2. So, heat loss due to radiation and exhaust flow is much larger than the cases diluted by either Ar or N_2. In order to sustain the flame, more fuel (hence higher equivalence ratio) is necessary for the flame using CO_2 as a diluent. It should be pointed out that when using CH_4 as fuel, CO_2 as diluent and O_2 concentration of 21%, the flame can not be ignited in this burner, even when the equivalence ratio is approaching one.

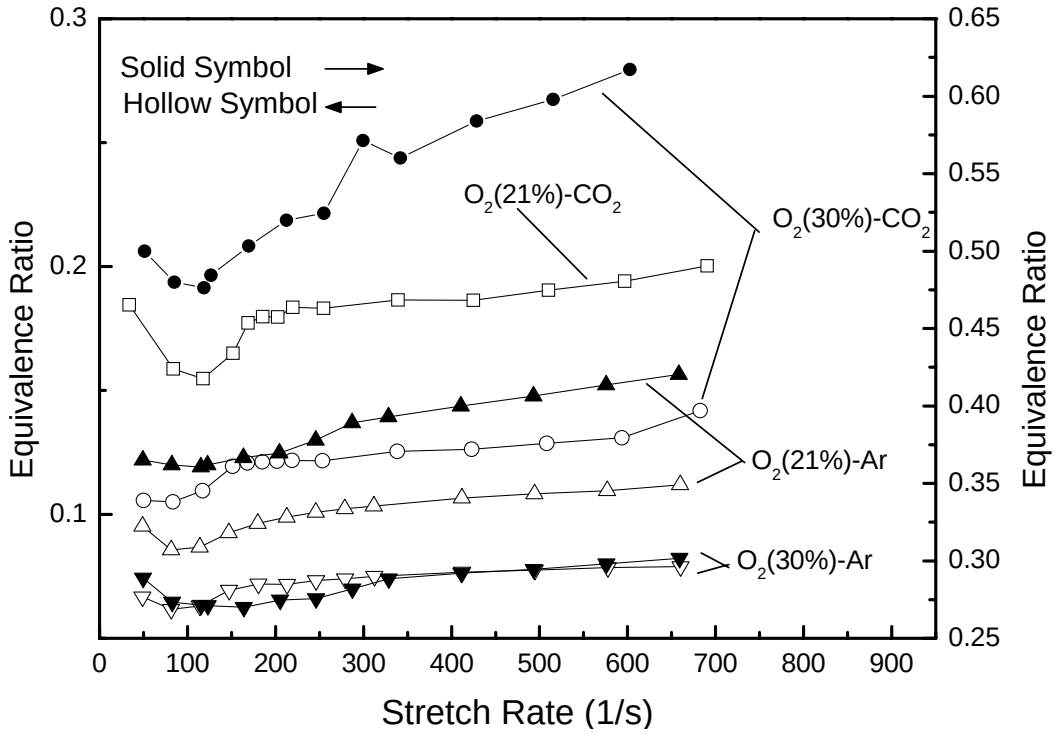

Figure 6. Extinction limit curves of H_2/O_2 flames (hollow symbol) and CH_4/O_2 flames (solid symbol) with diluted by Ar and CO_2 at same concentration

Cellular instability

Figure 7 shows the shape of the cross section of the hydrogen flame at various equivalence ratios. It is clear that the cellular instability appears when the hydrogen concentration is increased. The number of petals also increases gradually with equivalence ratio. The dark region between petals indicates local extinction. The onset condition for the two-petal cellular structure is non-distinctive, and therefore all reported data start with three petals.

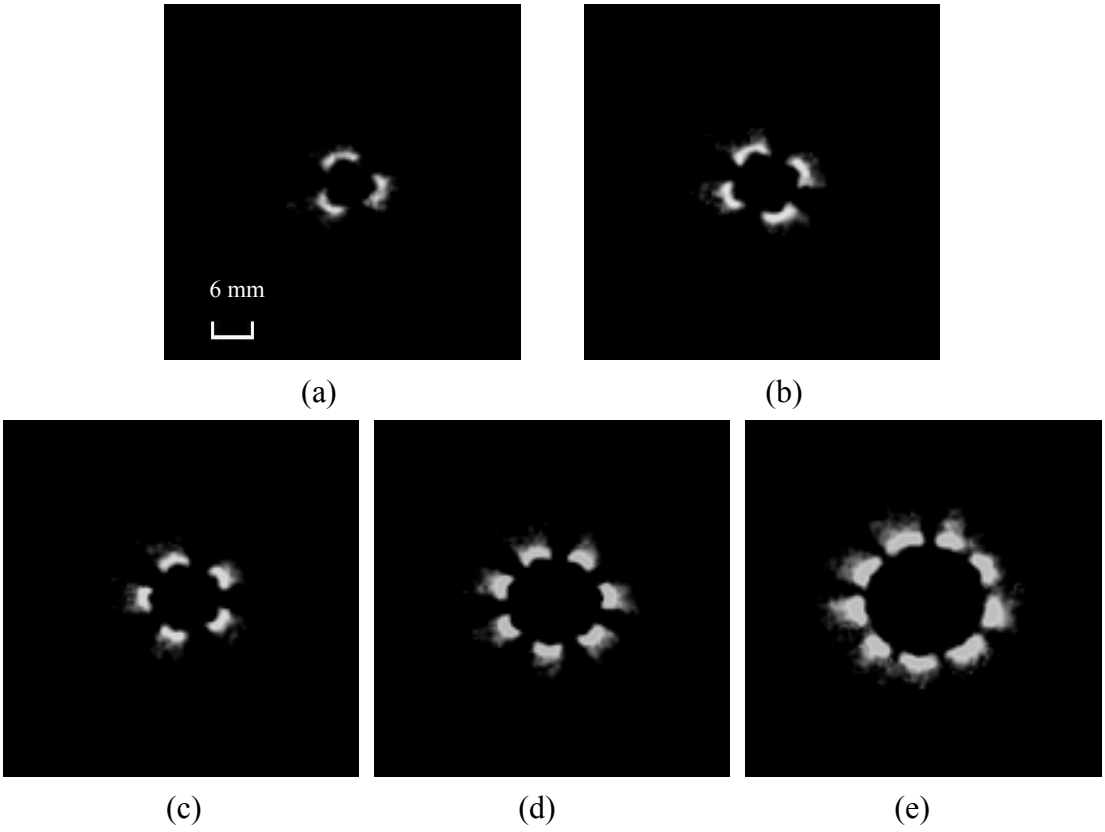

Figure 7. Cellular structure in premixed tubular flames of H_2/air:
(a) Φ=0.25, k=422 s^{-1} (b) Φ=0.27, k=434 s^{-1} (c) Φ=0.274, k=444 s^{-1}
(d) Φ=0.30, k=457 s^{-1} (e) Φ=0.336, k=472 s^{-1}

More interesting phenomena occur at the transition period. As the hydrogen flow rate is increased, the initially stable flame starts rotating. When it approaches certain level, one of the petals starts to vibrate, and then a new petal splits from the vibrating one. The new one is not stable, and sometimes merges back into its neighbors. Continuously increasing the hydrogen stabilizes the petals. The flame keeps rotating until the hydrogen concentration reaches a higher level. It then starts the next cycle to generate a new petal. In our present work, the onset point at which the flame shows a stable number of petals is recorded as the transition point.

Figures 8 and 9 show the maps of the multi-petal flame region in the plane of the

equivalence ratio and stretch rate. Star symbols indicate the extinction limit at different test conditions. Similar to the extinction experiments, at high stretch rate, the onset of the cellular instability occurs at higher equivalence ratio for flames diluted by CO_2 than those diluted by Ar.

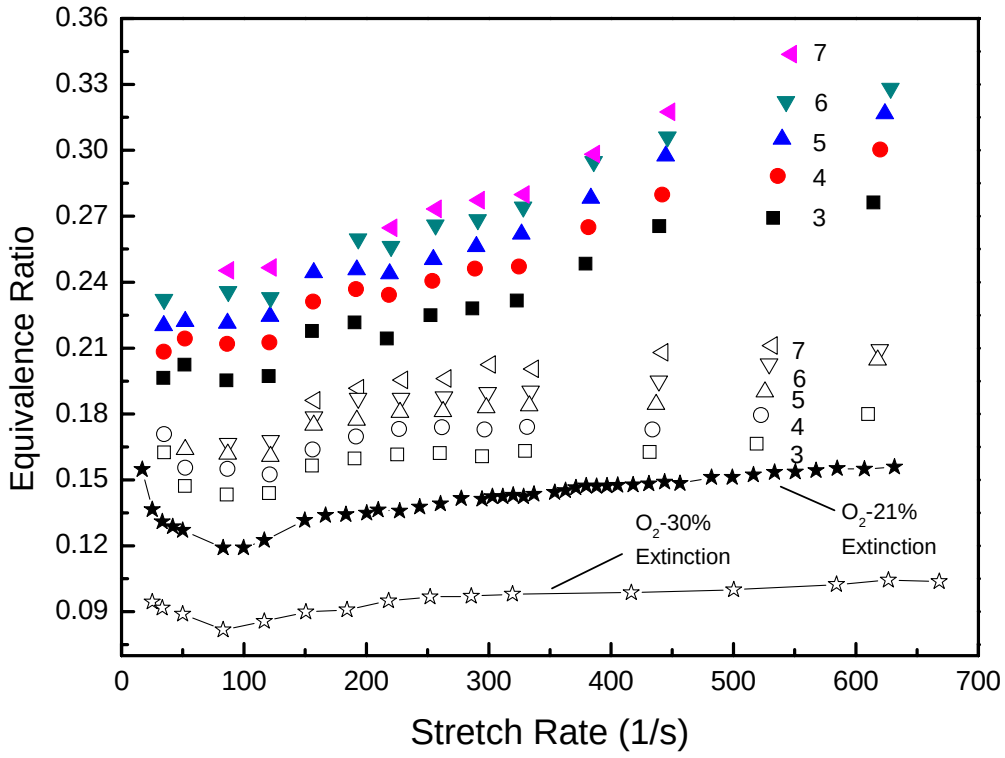

Figure 8. Plot of various regions of petal flames of hydrogen diluted with N_2 at 79% (solid symbol) and 70% (hollow symbol). Star symbols indicate the extinction limits.

According to a recent review by Law (2006), the instability phenomenon is the result of the combination of pure curvature effects, hydrodynamic instability, and thermal-diffusive instability. Pure flame curvature for equidiffusive flames with finite flame thickness will stabilize the flame surface due to the increase of the flame speed for concave curvature and the decrease of the flame speed for convex curvature. This curvature effect decreases with reduced flame curvature and reduced flame thickness.

The hydrodynamic instabilities are always unstable. For our case of Le<1 premixed flames, the diffusive-thermal effects are destabilizing as well (Law 2006). Since we do not observe petal formation and local extinction for nearly equidiffusive methane-air flames as discussed later, the dominate instability effect leading to petal formation is thermal-diffusive.

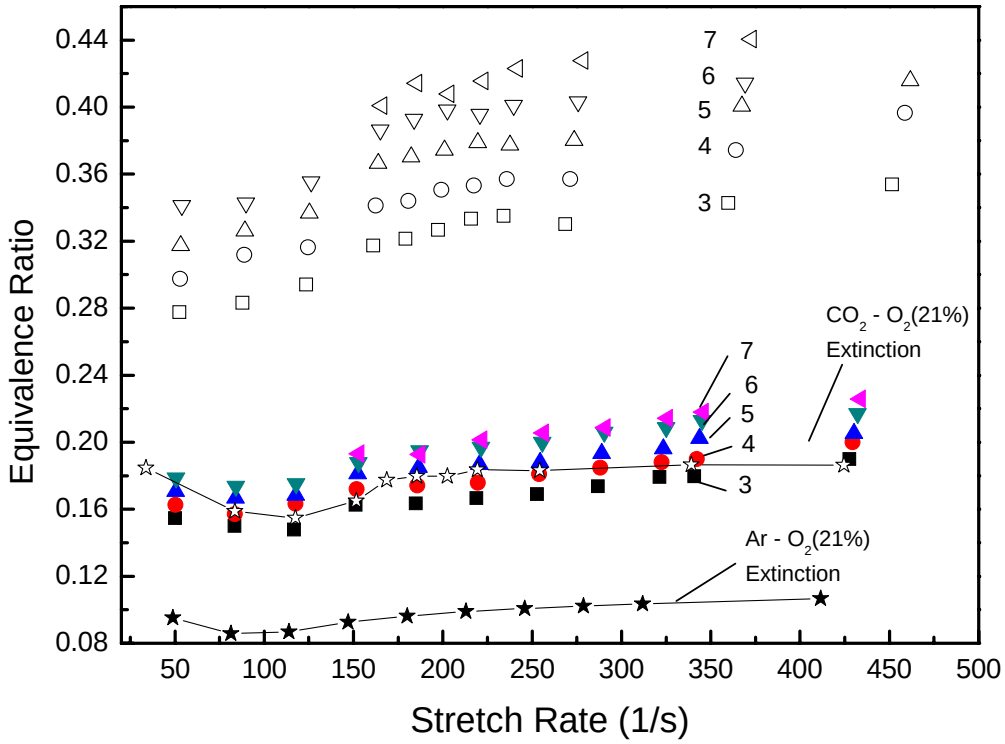

Figure 9. Plot of various regions of petal flames of hydrogen diluted with Ar (solid symbol) and CO_2 (hollow symbol) at 79%. The star symbols indicate the extinction limits

In our case, increasing the hydrogen concentration increases the flame speed, which means that the flame sheet will move towards the upstream region and the diameter of the tubular flame becomes larger. Eventually, the flame stabilizes at a larger radius where the flame speed is balanced with the radial component of the

inward flow. At the beginning of this process, instabilities triggered by hydrodynamic and diffusive-thermal effects are suppressed by the stabilization effect of pure curvature. As the diameter is increased, the pure curvature effect becomes less important due to the decreased curvature of the flame. When the diameter reaches a sufficient size to where diffusive-thermal and hydrodynamic instabilities dominate, the petal structure starts to form.

Moreover, the convex shape will intensify the flame, whose Lewis number is less than one. The smaller the radius of curvature is, the stronger flame becomes as it has an increased temperature (Mosbacher et al. 2002). That is why the lean hydrogen flame (Le<1) became a thin luminous rod when it approaches the extinction limit. In our case, when the petal structure appears, the radius of curvature of the petals is larger than that of the overall flame (see Figure 7). This convex-curved structure can therefore maintain the stability of each petal flamelet.

Lean methane flames also show cellular instability with increasing equivalence ratio despite that the Lewis number of methane mixture is just slightly less than one. Figure 10 shows the cross sectional shape at various concentrations and the flame becomes wrinkled as the fuel concentration is increased. We do not observe petal formation in lean methane flames due to the absence of strong thermal-diffusive effects for these nearly equidiffusive flames. Vertically-mounted rich propane-air tubular flames from Ishizuka (Le<1) also show cellular instabilities with distinct wrinkles (Ishizuka 1993).

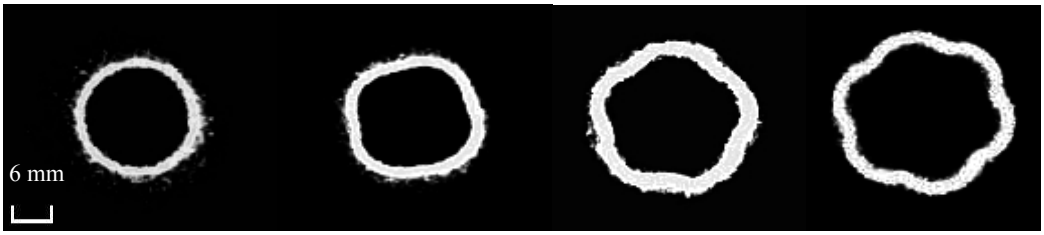

(a) (b) (c) (d)

Figure 10. Cellular structure in premixed tubular flames of CH_4/air:

(a) Φ=0.60, k=372 s^{-1}; (b) Φ=0.64, k=378 s^{-1};
(c) Φ=0.69, k=385 s^{-1}; (d) Φ=0.71, k=389 s^{-1}

Stretch, besides its influence on number of cell, also affects the cell distribution. In our case, the direction of stretch of premixed tubular flame is along the axis of the burner, which results in expanding or stretching the flamelet along this direction. Due to this effect, the dark region between two bright cells is always parallel to the axis, and the cells therefore are symmetrically spaced around the central axis, where the flame is least stretched. This cell distribution agrees with the "star" flame found by Lee and Sohrab (1995) where flame was stretched in radial direction but cells were distributed along the azimuthal coordinate.

A similar cellular flame structure was observed by Lo Jacono and Monkewitz (2007) for a non-premixed jet flame of CO_2-diluted H_2 jet fuel burning in a pure oxygen co-flow. In their work, the non-premixed flame instabilities show a different tendency when compared to the premixed tubular flame. Cells in the non-premixed jet flame show a smaller curvature (flatter flamelets) than those observed in the premixed tubular flame. They are also more likely to form under lower initial mixture strength conditions. Increasing H_2 concentration in the jet fuel mixture will turn petal-structure

flame back to a perfectly circular and continuous flame structure. At a certain condition, more than one state might co-exist, i.e. the flame shows a multiplicity on petal numbers. Such multiplicity is seldom observed in the premixed tubular flame except when the instability approaches the transition point. Even when multiplicity occurs in the tubular premixed flame, only two possible states are observed and the number of petals only differ by one, which is fewer than those observed in non-premixed jet flames where the number of petals can vary from 4 to 10 for the same flow condition. These contrasting observations show that the instability mechanisms in these non-premixed flames are fundamentally different from premixed flames.

Conclusion

A series of experiments are conducted to investigate the extinction and cellular instability of premixed tubular flames. Lean extinction limits of H_2 and CH_4 premixed tubular flames are reported for different stretch rates, diluents (N_2, CO_2, and Ar) and oxygen concentrations (21%, and 30%). Cellular structures are observed for H_2 flames with small Lewis numbers that are tuned away from extinction. The combined effects of thermal-diffusive instability and hydrodynamics instability are believed to induce the cellular instability occurred in this flame. The effect resulting from pure curvature inhibits the onset of the instabilities. A brief comparison about the structure of the premixed tubular flame and the non-premixed jet flame shows that their instabilities are driven by different mechanisms.

CHAPTER III

CELLULAR INSTABILITY IN NON-PREMIXED OPPOSED TUBULAR FLAMES

Introduction

In this chapter, we study the cellular instability of non-premixed opposed tubular flames. Instability phenomenon has been observed by many researchers with different non-premixed flame burners and experimental conditions. With a slot burner, Chen et al. (1992) proposed that the non-premixed flame with sufficiently low effective Lewis number exhibit cellular instability only near extinction. This conclusion was confirmed by Lo Jacono et al. (2003) in their study, which was carried on an axisymmetric jet (AJ) burner. They reported when H_2 and CH_4 were diluted by N_2, CO_2, Ar, He and SF_6, a strong dependency of cellular state on initial mixture strength (the initial mixture strength is defined as the fuel to oxygen ratio normalized by the stoichiometric ratio) was found, which was that the cell length and number increases with initial mixture strength increasing and Damköhler number (ratio of characteristic mixing time to chemical reaction time) decreasing. Using the same AJ burner and another Woflhard-Parker (WP) jet burner Lo Jacono and Monkiwitz (2007) found the multiplicity of cellular state for non-premixed flame and mapped the cell-structure states on the space of parameters. Meanwhile, initial mixture strength and Lewis number once again showed their influence on cell structure. Further, a one-dimensional unstrained planar non-premixed burner was designed by Lo Jacono

et al. (2005). They found that cellular instability is more prevalent at low initial mixture strength and Lewis number. Based on these data, Frouzakis et al. (2005) successfully repeated this process with a 3-D numerical simulation in which cellular instability appeared with decreasing fuel or oxidizer Lewis number and Damköhler number. Metzener and Matalon (2006) illustrated the instability modes in the fuel-oxidizer Lewis number parameter plane. Their work indicates both Lewis numbers in fuel and oxidizer strictly less than one is not a necessary condition for the onset of cell instability. Later, Matalon (2007) reviewed those instabilities of non-premixed flames which were carried on different burners and with various fuel, oxidizer and diluent gases. His review indicates that this phenomenon appeared when the Lewis number on the fuel side is smaller than one.

The effect of curvature and stretch on non-premixed flames and their instability has also been studied. Wang et al. (2006) derived the stretch rate formulation on opposed the tubular non-premixed flame, and investigated the effect of stretch and curvature. Wang et al. (2007) found that positive curvature (the flame is convex to the fuel flow) enhanced preferential diffusion and, vice versa for negative curvature. The strengthening and weakening effect is proportional to the ratio of flame thickness to flame radius. Hu et al. (2007b) confirmed these effects experimentally, showing that for flames with fuel Lewis number less than one that convex curvature towards the fuel promotes combustion and vice versa for concave curvature.

Hu (2007a and 2008) used an opposed tubular burner to investigate the onset of cellular instability and extinction behavior of opposed non-premixed tubular flame.

His study confirmed Wang's finding about the curvature effect. Nevertheless, the onset condition characterizing the different number of cells was not mentioned in this study.

The main purpose of this work is to study the process of cellular formation in opposed tubular non-premixed flames, from cell origin, developing to final extinction, especially, the onset points of each different cellular states and the dependency of cell length on experimental conditions. These data could be used to further investigate the effect of stretch, initial mixture strength and curvature both experimentally and numerically.

Experimental Setup

All experiments were conducted in the same tubular burner used in Chapter II and reported earlier (Wang et al. 2008a and 2008b). Compared to the former premixed tubular configuration, a quarter-inch-diameter (6.35mm) porous-made inner nozzle was carefully mounted through the burner, so, an opposing flow field could be established as shown in Figure 11. More detail was reported in Wang et al.. (2008a and 2008b). The effect of curvature depends on preferential diffusion in either the oxidizer stream and/or the fuel stream. Since the Lewis number of the oxidizer is near one (Le_o=1) the effect of curvature only depends on the fuel stream. Here we will define curvature convex to the fuel stream as positive and concave to the fuel stream as negative. In this study, all fuel flow is induced through the inner nozzle, and oxidizer is from the outer nozzle so, the flame is always concave to the fuel side flow.

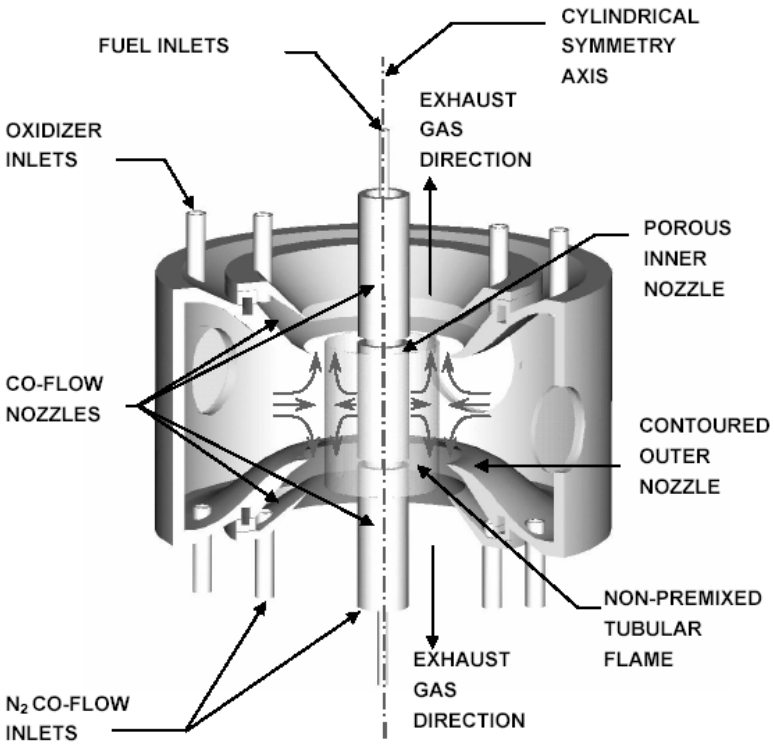

Figure 11. Opposed non-premixed burner structure

A mirror with a slot-cut is mounted underneath the tubular burner at 45 degrees to axis of symmetry, which provides a view of the flame in the axial direction. The same infrared sensitive ICCD video camera (Xybion ISG-250 with scan rate 60Hz) mentioned in Chapter II is applied here also. It is mounted horizontally toward the mirror records the axially-integrated chemiluminescence emission form the flames to monitor the extinction and cellular structure. A sample image of a stable tubular flame is shown in Figure 12a. Due to the blockage from inner nozzle, the upper part of the flame image is weaker than the rest.

All gas flows are controlled by mass flow controllers (Teledyne Hastings HFC 202/203) through a computer. During experiment, we ignited the tubular flame at low

air flow rate, and then increased the air flow rate slowly (0.3-0.5% of total range each step) until the flame reached extinction.

The definitions of stagnation radius and stretch rate of a cold opposed tubular flow, R_s and K, are given by Wang et al. (2007), which are both dependent on the inlet radii R_i, gas densities ρ_i and velocities V_i of the flow opposing streams, where i=1 is the inner nozzle and i=2 is the outer nozzle (see Figure 1).

$$R_s = R_2 \cdot \left[1 - \frac{\frac{R_2}{R_1} - \frac{R_1}{R_2}}{\frac{R_2}{R_1} - \sqrt{\frac{\rho_1}{\rho_2}} \cdot \frac{V_1}{V_2}} \right]^{0.5} \quad (1) \qquad K = \pi \cdot \frac{V_1}{R_1} \cdot \left[\frac{\frac{V_2}{V_1} \cdot \frac{R_2}{R_1} \cdot \sqrt{\frac{\rho_2}{\rho_1}} - 1}{\frac{R_2^2}{R_1^2} - 1} \right] \quad (2)$$

Experiment Procedures and Results

A series of thirty-one experiments with different diluents and different concentration were conducted in this burner. On the fuel flow side, the gas composition is H_2 diluted with CO_2, He, N_2 or Ar, respectively. The oxidizer is air only. The mole ratio of H_2 to the diluents could be varied. For one certain ratio, the cases with different total flow rate of fuel composition were repeated to investigate the cellular instability. A summary of the detailed conditions are listed in Table 2.

Table 2. List of experimental conditions for non-premixed opposed tubular flames

Fuel Side Composition	Mole Ratio of H_2 to Diluents	Total Fuel Side Flow Rate (SLPM)	Oxidizer Flow Rate (SLPM)	Mole-based Initial Mixture Strength $\times 10^{-2}$	Lewis Number In Fuel Side
H_2/CO_2	5 : 13	0.72 - 1.26	28.3 - 82	1.02 - 1.68	0.414
	5 : 18	0.92 - 2.76	10 - 85	1.68 - 14.28	0.351
H_2/N_2	5 : 13	0.72 - 1.08	38.6 - 88.6	0.81 - 1.23	0.547
	1 : 5	1.2 - 4.2	26 - 80	1.40 - 2.92	0.424
H_2/Ar	5 : 13	0.72 - 0.99	50 - 95.2	0.69 - 0.95	0.564

For any of cases above, the flame was ignited at low air flow rate. Initially, the flame image showed a perfect circle, as shown in Figure 12(a), with the air flow rate increasing, gaps (dark region between two bright zones, which is a local extinction region) appeared one by one, which split the flame circle into a cellular (multi-petal) structure until the number of cells reached maximum. Further increasing the air flow rate would result in shrinking the length of each cell and enlarging the dark regions (gaps). The flame intensity became weaker and weaker. When the air flow rate reached certain level, some cells began to extinguish. The number of cells would continue decreasing until the flame extinguished. Figure 12 (a)-(k) showed this process where the maximum cell number is 5. The maximum number of cells seems to depend on the flow rate of fuel. Increasing the fuel flow rate causes more cells to form. Figure 12 (l), (m) show this dependence on fuel flow rate as 12(m) has a higher fuel flow rate. Here, it should be noticed that Figure 12(l) and 2(f) have same cell number, but the length of cells is different. Since these states are fundamentally different, the letter S (short) and L (long) were used to distinguish them, e.g. Figure

12(d) 4L and Figure 12(g) 4S.

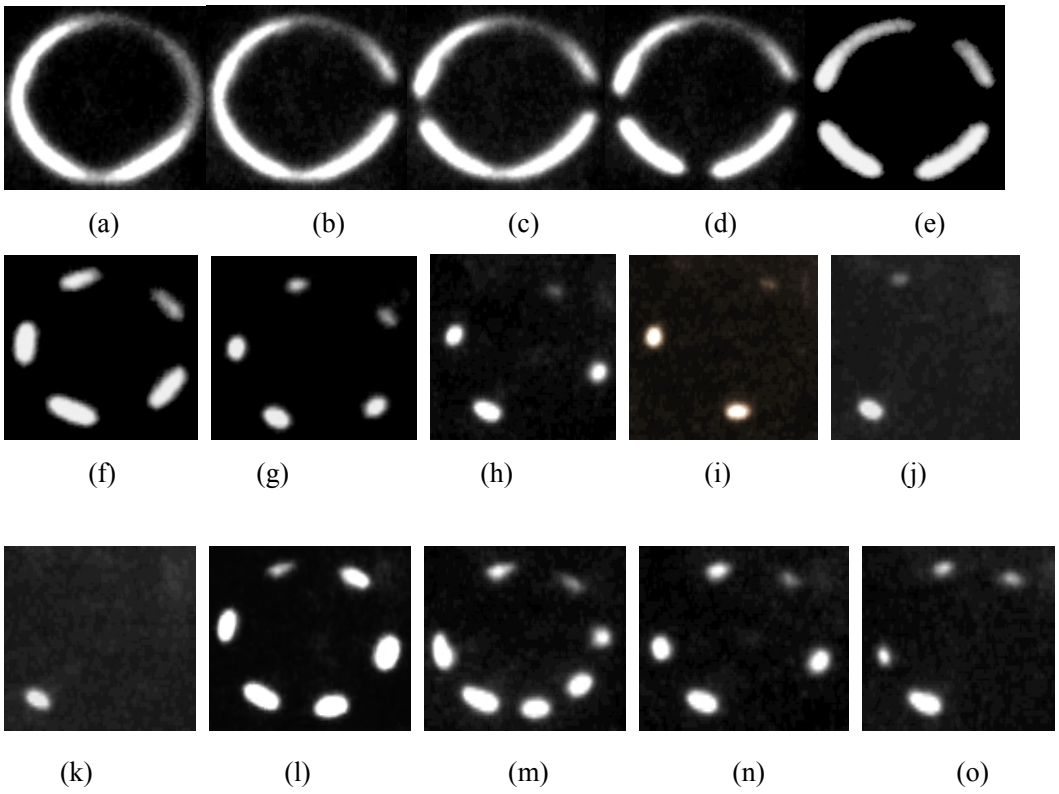

Figure 12. Cell Structure in formation in positive process with constant fuel flow rate and increasing air flow. Fuel: H_2 (0.35 slpm) diluted with CO_2 (1.26 slpm); Oxidizer: Air

(a) Φ=0.0833, k=60.0 s^{-1} (b) Φ=0.0793, k=68.0 s^{-1} (c) Φ=0.0724, k=75.8 s^{-1}
(d) Φ=0.0666, k=83.6.0 s^{-1} (e) Φ=0.0505, k=114.7 s^{-1} (f) Φ=0.0309, k=196.4 s^{-1}
(g) Φ=0.0225, k= 274.3 s^{-1} (h) Φ=0.0186, k=336.6 s^{-1} (i) Φ=0.0185, k=337.3 s^{-1}
(j) Φ=0.0184, k=338.1 s^{-1} (k) Φ=0.0183, k=339.7 s^{-1} (l) Φ=0.0397, k=176.1 s^{-1}
(m) Φ=0.0216, k=451.1 s^{-1} (n) Φ=0.0203, k=350.2 s^{-1} (o) Φ=0.0193, k=507.8 s^{-1}

Generally, the flame cells are stable and do not change their spatial position as the air is increased, but sometimes unstable behavior also appeared. There were a few cases in which cells showed a spontaneous location adjustment at transition points. Generally, as the air flow was increased further, the cells were symmetrically distributed around the inner nozzle. Nevertheless most of cases did not move after other cell extinguished. This made the structure non-uniform, such as shown in Figure

12 (n) and (o).

During the process mentioned above, the fuel flow rate is fixed but the air flow rate is increased monotonically which we call a “positive” process. The flame state with a maximum number of cells kept a fairly long time in this process. Compared with this state, other states only existed for a shorter time, and only occurred at the early and late period. Especially when the flame approached extinction, the number of cells became very sensitive to the air flow, even though each step only increased the air flow rate by 0.2% of the total range. Such an increment usually caused the number of cells to sharply drop to states with 4, 3, 2 cells or 1 cell, even extinction.

On the other hand, the “negative” process when the air flow rate is monotonically decreased showed a different process from the “positive” process. As mentioned above, a drop of cell number from the maximum could be induced at high air flow rate. Right after some cells started to disappear, decreasing air flow rate would not lead the disappeared one to recover immediately. Flame cells would stay in its latest state. As air flow rate decreased further, each of them was strengthened in its length, width. As Figure 13 shows, this process would continue until the air flow was low enough so that the cell structure flame was changed to a new state with longer cells, even directly jumping to the state with maximum cells.

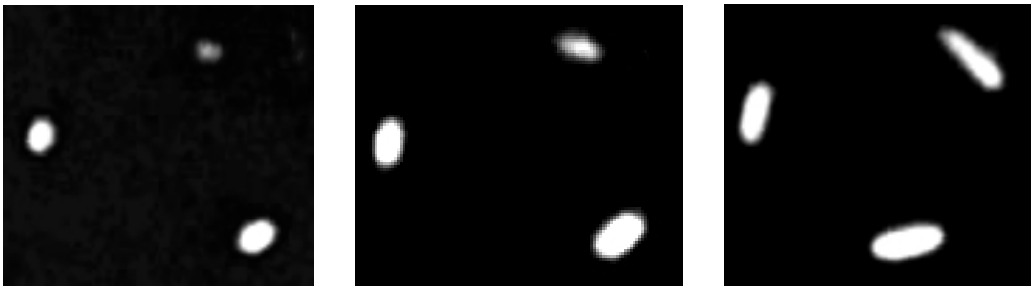

(a) (b) (c)

Figure 13. Cell structure in "negative" process. Fuel: H_2 (0.25 slpm) diluted with CO_2 (0.9 slpm); Oxidizer: Air

(a) Φ=0.0192, k=211.8 s^{-1} (b) Φ=0.0238, k=169.7 s^{-1} (c) Φ=0.0283, k=140.6 s^{-1}

Both "positive" and "negative" processes are illustrated in Figure 14. Three transition zones are marked separately. In a positive process, the number of cells increase in Zone I(P) and the maximum number of cells is held until Zone II(P) when the cell numbers rapidly decreases. As the air flow rate is decreased from Zone II, the number of cells is held until Zone III(N). Zone III(N) shows that when the transition takes place, the flame tends to generate as many cells as possible. As the air flow is decreased, the potential is accumulated further until a tiny disturbance occurs, the flame would jump to a state which could release the potential which could no longer be suppressed. This disturbance could be in any of form, such as a tiny uniformity in flow field. Because of the unpredictable disturbance, the transition of flame structure could be triggered prior to the limit condition. That is why in Figure 13 under a negative process the 1-cell state has two transition points where it jumped back to different states. In addition, the 2-cells state shows two possibilities at almost the same transition point.

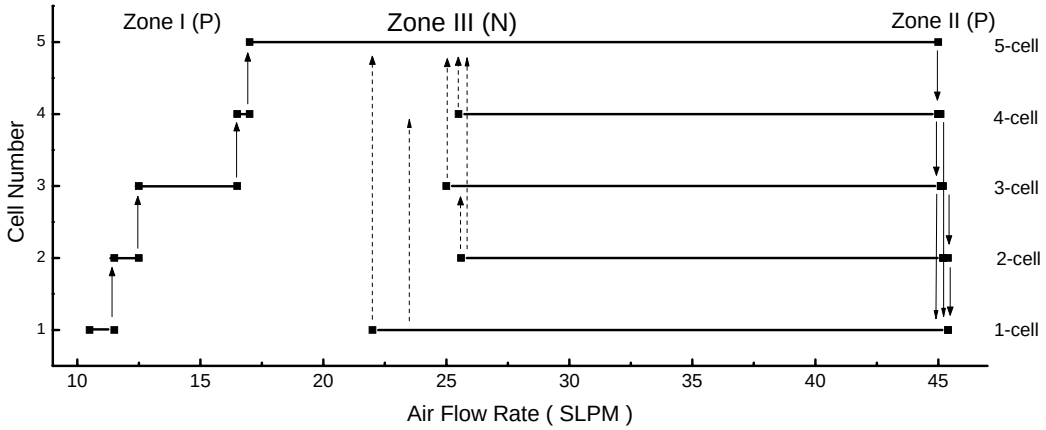

Figure 14. Transition map of cell structures Fuel: H_2 (0.35 slpm) diluent with CO_2 (1.26 slpm); Oxidizer: Air

Similar sensitive dependency on air flow rate appears in Zone II(P), where the flame is very weak due to stretch and heat loss to inner nozzle. So a small change in parameter space will cause an obvious change in cell numbers. This trend agrees with Lo Jacono et al. (2003, 2005 and 2007) and the Frouzakis et al. (2005) study, where introduction of bluff bodies even noise were applied as perturbation of the flow field to induce state transition.

Different from these two Zones, in Zone I(P), transitions points are relatively fixed. The range between two transition points is more apparent. This is mainly because flame was strong enough to overwhelm the negative effects caused by any weak disturbance. Only as the disturbance is strong enough does the flame change its structure. Another difference is that the cell in Zone I is larger and longer than the cell in Zone II and III. Due to the difference in driving cell generation, the transition points in Zone I are more repeatable than those in Zone II and III.

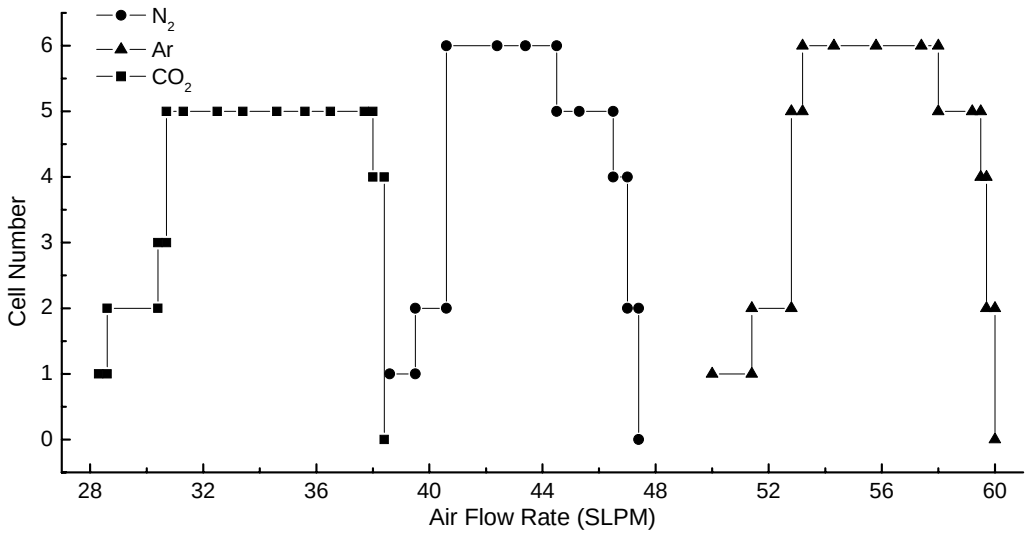

Figure 15. Transition map (positive) of cell structures with different diluents. Fuel: H_2 (0.2 slpm) diluted with CO_2, N_2 and Ar (0.52 slpm respectively); Oxidizer: Air

Experiments with different diluents at different concentration were also conducted. Figure 15 shows the transition map (positive) for the H_2 flame (0.2 slpm) diluted with CO_2, N_2 and Ar (0.52 slpm respectively). It shows similar profiles for the three cases, the only difference is the position shift. The case diluted with CO_2 starts the transition process at a lower air flow rate than those diluted with N_2 and Ar. The possible reason is that CO_2 has the largest specific heat among these three diluents. So a lower air flow rate is sufficient to trigger the CO_2-case to start this process.

Similar shift occurred in the cases diluted with the same gas but at a different concentration. Figure 16 shows the transition map of H_2 diluted with CO_2 with mole ratio 5:18. It shows the case with higher hydrogen concentration started its transition process at higher air flow rate, which means lower initial mixture strength. This further confirmed the phenomenon and conclusions discussed before.

Besides the initial mixture strength, Lewis number of fuel flow is another important influence on cellular instability. The Le_f in above experiments ranges from

0.413-0.533. The case in which Le_f is greater than 1, for example H_2 diluted with helium, was repeated with the same procedure. The flame did not show any cell or stripped structure even until it reached complete extinction.

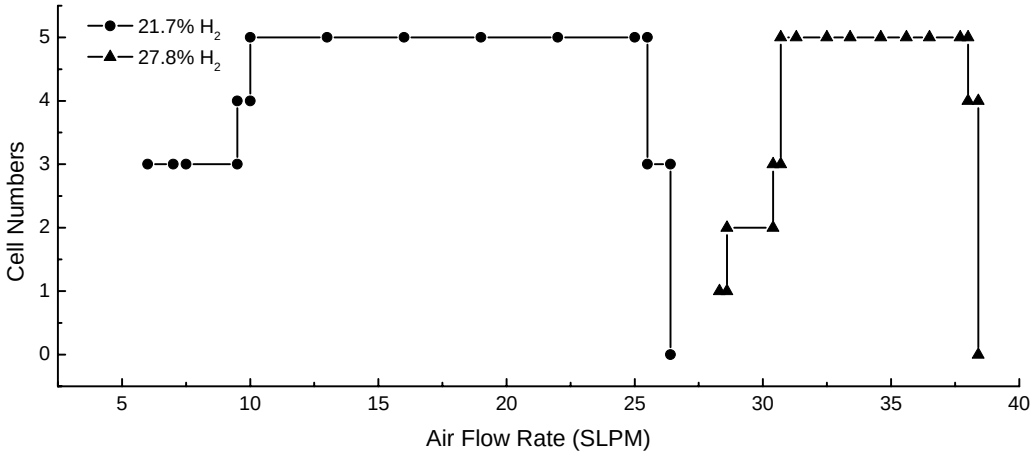

Figure 16. Transition map (positive) of cell structure with different diluted concentration. Fuel: H_2 (0.2 slpm) diluted with CO_2 at 0.52 slpm (square symbol) and 0.72 slpm (round symbol); Oxidizer: Air

Results and Discussion

Cell number

All the experiments once more confirmed the effect of initial mixture strength and Lewis number on cellular instability in opposed tubular flame. Also the curvature effect could play a role here. But these effects on the cell appearance are coupled together in the experimental procedure where the fuel flow rate is fixed and the air flow rate is increased. The dependency of cell number on only one parameter variation is needed.

According to equation (1) and (2), we can find that R_s and K and initial mixture

strength Φ are the function of the parameter of flow rate.

$$R_s = f\left(\frac{\rho_1}{\rho_2}, \frac{V_1}{V_2}\right), \qquad K = f\left(V_1, R_1, \frac{V_1}{V_2}, \frac{\rho_1}{\rho_2}\right), \qquad \Phi = f\left(\frac{V_1}{V_2}\right)$$

So, if we can set these parameters properly, it is possible that we can get a series of experimental points where only stretch rate has been changed but stagnation radius and initial mixture strength are kept constant. The thirty-one experiments were reorganized into new groups of constant initial mixture strength and stagnation radius, where the only two varied parameters were stretch and cell number. Some cases were picked out in Figure 17 to demonstrate this relationship.

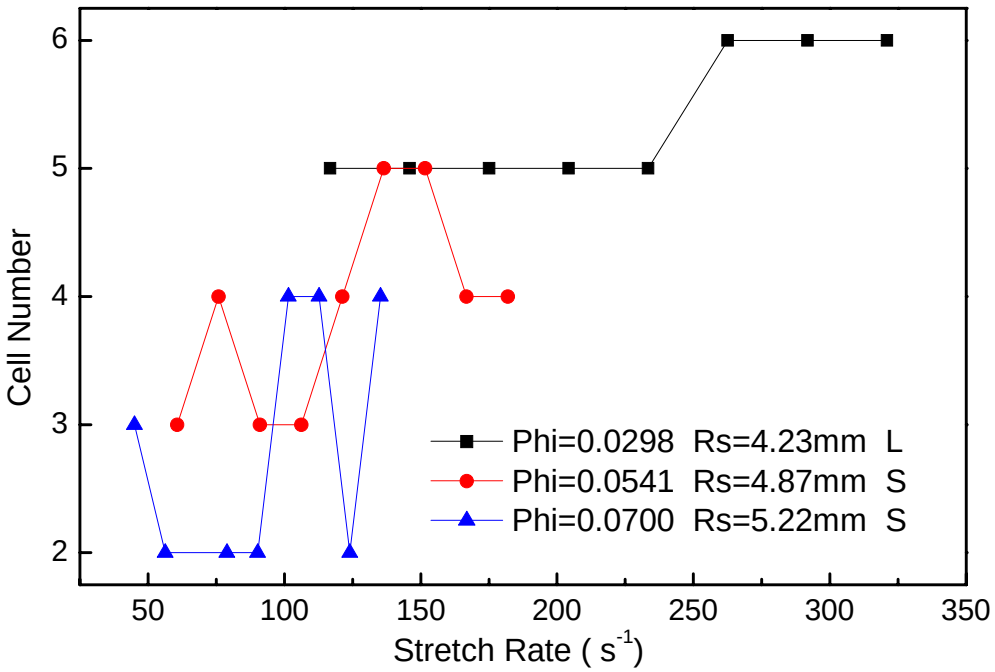

Figure 17. Cell number vs. stretch with reorganized data

Unfortunately, these data do not show a consistent tendency in terms of cell number or length. The results do not agree with any theoretical expectation. The

possible reasons include the imperfect apparatus and multiplicity of states. From the Figures 15-17, it has been noticed that the state with maximum cell number stayed for the longest period in each ease. This is not caused by the parameters only, but also the air flow rate increment in each step. As Lo Jacono et al. (2007) found in their study, the flame would change its cellular structure into a different one according to the induced disturbance. This judgment has been confirmed in our study by conducting a positive process with larger air flow rate increment in each step. In this situation, the transition points would be shift to a lower condition with a larger step.

In order to avoid the influence caused by this indirect experimental procedure, three groups of experiments where fuel flow rate, diluent flow rate and air flow rate are simultaneously changed are conducted. The results are shown in Figure 18.

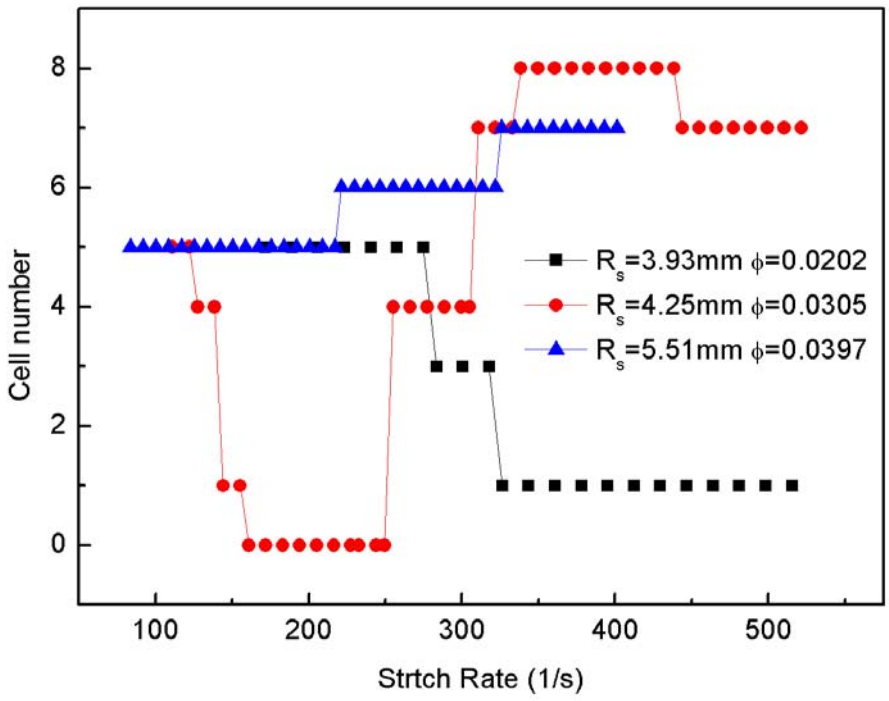

Figure 18. Cell number vs. stretch

Similar to Figure 17, Figure 18 does not show a consistent dependency of cell number on stretch rate either. For the case with the smallest stagnation radius and initial mixture strength, the cell number decreases with stretch rate increasing, but for the case with the largest stagnation radius and initial mixture strength, the results show a reversed trend. Moreover, the middle case has no fixed trend with stretch rate at all. More detailed work is needed.

Cell Length

Cell length is another parameter studied in this work. The cell length is measured with the pictures taken with the ICCD camera at specific conditions. Like those in above discussion about cell number, the chosen conditions in this section are also those with same initial mixture strength and stagnation radius but different stretch rate. The detail results are shown in Figure 19.

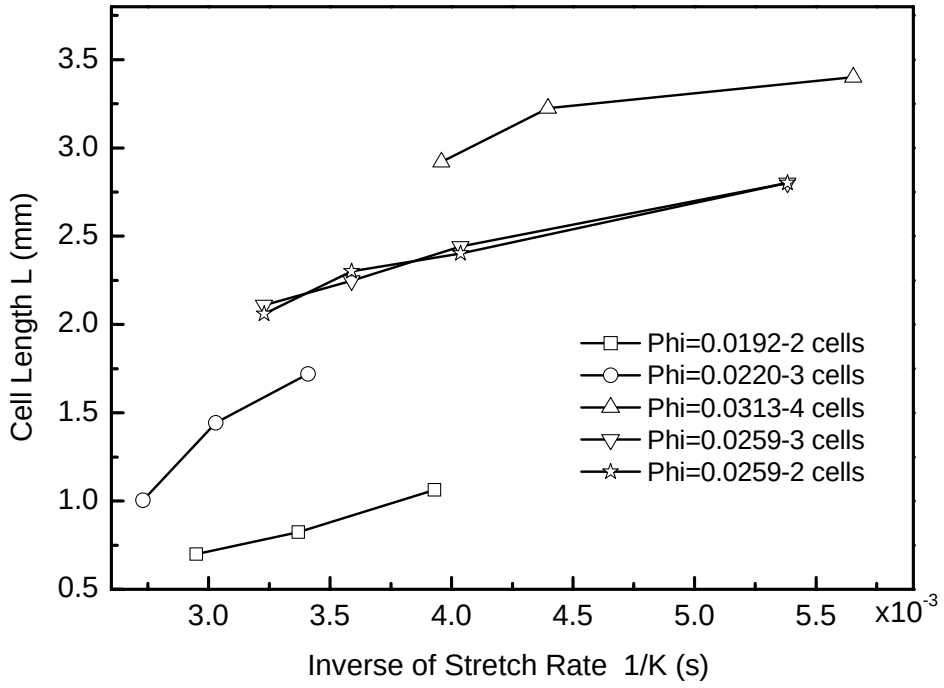

Figure 19. Cell length vs. inverse of stretch rate. H_2 (diluted with CO_2)-Air flame

Each case shows a trend that cell length increases with stretch rate decreasing. Even for the multiplicity cases (Φ=0.0259) with 3 cells and 2 cells (indicated by inverse triangle and star symbol separately), such a trend still applies. Similar results were found by Lo Jacono et al. (2007), where the cell length is smaller at higher Reynolds Number. Damköhler number provides a possible reason for this trend. In our case, according to the definition of stretch rate, larger stretch rate means higher velocity which results in a smaller characteristic mixing time for the flame. Consequently, cell length will be diminished due to time deficiency of the combustion reaction.

Besides the stretch rate, initial mixture strength seems to be another parameter significantly influencing the cell length. The cell length shows an obvious change with initial mixture strength increasing, but for the cases with same initial mixture strength (Φ=0.0259), the change is almost indistinguishable. This, once again,

confirmed our conclusion on this parameter.

Conclusions

A series of non-premixed opposed tubular flame experiment have been conducted on cellular instability. The cellular instability and transition points have been found and carefully recorded. The hydrogen flame diluted by CO_2, N_2 or Ar shows this phenomenon only occurred when the flame approaches extinction, which indicates that the initial mixture strength played an important role here. But a similar structure has never happened for the He diluted flame. This proved influence of Lewis number on cell structure, the detailed quantitive analysis about the dependency of cell number on experimental parameters is still needed to be done. Cell length is another parameter studied in this work. The decreased Damköhler due to increased velocity is the main reason for the cell length shrinking.

CHAPTER IV

SUMMARY AND FUTURE EFFORTS

This study demonstrates the behavior of cell instability and extinction phenomenon in premixed tubular flames and non-premixed opposed tubular flames. The results agree with the previous experimental data acquired in other types of premixed and non-premixed flames by other researchers. A detail analysis confirmed that Lewis number, equivalence ratio (for premixed tubular flames), initial mixture strength (for non-premixed opposed tubular flames) curvature effect and Damköhler number played significant roles in both premixed and non-premixed flames. Since the cell structure is only observed in the flames whose Lewis numbers are less than one; the Lewis number is still a major factor to cellular instability in premixed and non-premixed flames. The ratio of fuel to oxidizer took different effects on both cases. For lean premixed flames, cells were only found in the conditions where equivalence ratio is high enough, and the number of cell increased with increasing equivalence ratio. Nevertheless, for the non-premixed case, they were only observed in the conditions close to extinction, and increasing the initial mixture strength would reform the flame from a cellular structure to a circle.

Compared to the premixed tubular flame, non-premixed opposed tubular flame showed another unique property, multiplicity of states, where more than one kind of cell structure or “states” could possibility exist at a specific experimental condition.

This finding agrees with previous work in other burners. The intrinsic mechanism to this phenomenon is not still very clear, although a few of experimental results could be repeated well with numerical simulation. But much work is still needed to find the real physical mechanism behind this phenomenon.

REFERENCES

Chen, R.H., Mitchell, G.B. and Ronney, P.D. (1992) Diffusive-thermal Instability and Flame Extinction in Nonpremixed Combustion. *Proc. Combust. Inst.*, **24**, 213-221.

Frouzakis, C.E., Tomboulides, A.G., Papas, P., Fischer, P.F., Rais, R.M., Monkewitz, P.A. and Boulouchos, K. (2005) Three-Dimensional Numerical Simulations of Cellular Jet Diffusion Flames. *Proc. Combust. Inst.*, **30**, 185-192.

Hu, S., Wang, P., and Pitz, R.W. (2006) A Structural Study of Premixed Tubular Flames. 44th AIAA Aerospace Science Meeting and Exhibit, Paper No. AIAA-2006-0160, Reno, NV.

Hu, S., Pitz, R.W. and Wang, Y. (2007a) Extinction and Near-extinction Instability of Non-premixed Tubular Flames. 45th AIAA Aerospace Sciences Meeting and Exhibit, AIAA-2007-0177, Reno, Nevada.

Hu, S., Wang, P., Pitz, R.W. and Smooke, M.D. (2007b) Experimental and Numerical Investigation of Non-Premixed Tubular Flames. *Proc. Combust. Inst.*, **31**, 1093-1099.

Hu, S., Pitz, R.W., and Wang, Y. (2008) Extinction and Near-Extinction Instability of Non-Premixed Tubular Flames, *Combustion and Flame*, Accepted.

Ishizuka, S. and Law, C.K. (1982) An Experimental Study on Extinction and Stability of Stretched Premixed Flames. *Proc. Comb. Inst.*, **19**, 327-335.

Ishizuka, S. (1984) On the Behavior of Premixed Flames in a Rotating Flow Field: Establishments of Tubular Flame. *Proc. Combust. Inst.*, **20**, 287-294.

Ishizuka, S. (1989) an Experimental Study on Extinction and Stability of Tubular Flames. *Combust. Flame*, **75**, 367-379.

Ishizuka, S. (1991) Determination of Flammability Limits Using a Tubular Flame Geometry. *J. Loss Prev. Process Ind.*, **4**, 185-193.

Ishizuka, S. (1993) Characteristics of Tubular Flames. *Proc. Energy Combust. Sci.*, **19**, 187-226.

Jacono, D.Lo., Papas, P. and Monkewitz, P.A. (2003) Cell Formation in Non-Premixed, Axisymmetric Jet Flames Near Extinction. *Combust. Theory Modelling*, **7**, 635-644.

Lo Jacono, D., Papas, P., Matalon, M. and Monkewitz, P.A. (2005) An Experimental Realization of an Unstrained, Planar Diffusion Flame. *Proc. Combust. Inst.*, **30**, 501-509.

Lo Jacono, D. and Monkewitz, P.A. (2007) Scaling of Cell Size in Cellular Instabilities of Nonpremixed Jet Flames. *Combust. Flame*, **151**, 321-332.

Ju, Y., Matsumi, H., Takita, K. and Masuya, G. (1999) Combined Effects of Radiation, Flame Curvature, and Stretch on the Extinction and Bifurcations of Cylindrical CH_4/Air Premixed Flame. *Combust. Flame*, **116**, 580-592.

Law, C.K. (1988) Dynamics of Stretched Flames. *Proc. Combust. Inst.*, **22**, 1381-1402.

Law, C.K. and Sung, C.J. (2000). Structure, Aerodynamics, and Geometry of Premixed Flamelets. *Proc. Energy Combust. Sci.*, **26**, 459-505.

Law, C.K. (2006) Combustion Physics, First Edition, Cambridge, New York.

Lee, H. and Sohrab, S.H. (1995) "Star-Shaped Premixed Flames and Spatially Periodic Velocity Fields in Axisymmetric Counterflows, Eastern States Section Meeting of the Combustion Institute, Worchester Polytechnic Institute, Worcester, MA.

Lee, H. and Sohrab, S.H. (1995) Hydrodynamic Aspects of Premixed Flame Stripes in Two-Dimensional Stagnation-Point Flows. *Combust. Flame*, **101**, 441-451.

Matalon, M. (2007) Intrinsic Flame Instabilities in Premixed and Non-premixed Combustion. *Annual Review of Fluid Mechanics*, **39**, 163-191.

Metzener, P. and Matalon, M. (2006) Diffusive-Thermal Instabilities of Diffusion Flames: Onset of Cells and Oscillations. *Combust. Theory Modeling*, **10**, 701-725.

Mosbacher, D.M., Wehrmeyer, J.A., Pitz, R.W., Sung, C.J. and Byrd, J.L. (2002) Experimental and Numerical Investigation of Premixed Tubular Flames. *Proc. Combust. Inst.*, **29**, 1479-1486.

Sakai, Y. and Ishizuka, S. (1992) Extinction Characteristics of Tubular Flames Diluted with Nitrogen in a Rotating Stretched Flow Field. *Proc. Combust. Inst.*, **24**, 153-159.

Wang, P., Wehrmeyer, J.A. and Pitz, R.W. (2006) Stretch Rate of Tubular Premixed Flames. *Combust. Flame*, **145**, 401-414.

Wang, P., Hu, S. and Pitz, R.W. (2007) Numerical Investigation of the Curvature

Effects on Diffusion Flames. *Proc. Combust. Inst.*, **31**, 989-996.

Wang, Y., Hu, S., Pitz, R.W. (2008a) Extinction and Cellular Instability of Premixed Tubular Flames. 46th AIAA Aerospace Sciences Meeting and Exhibit, AIAA-2008-0979, Reno, Nevada

Wang, Y., Hu, S. and Pitz, R.W. (2008b) Extinction and cellular Instability of Premixed Tubular Flames. *Proc. Combust. Inst.*, **32**, Accepted.

Williams, F.A. (1981) A Review of Flame Extinction. *Fire Safety Journal*, **3**, 163-175.